



UNIVERSITY OF LEEDS

This is a repository copy of *Information length as a new diagnostic in the periodically modulated double-well model of stochastic resonance*.

White Rose Research Online URL for this paper:
<http://eprints.whiterose.ac.uk/144481/>

Version: Accepted Version

Article:

Hollerbach, R, Kim, E-J and Mahi, Y (2019) Information length as a new diagnostic in the periodically modulated double-well model of stochastic resonance. *Physica A: Statistical Mechanics and its Applications*, 525. pp. 1313-1322. ISSN 0378-4371

<https://doi.org/10.1016/j.physa.2019.04.074>

© 2019 Published by Elsevier B.V. Licensed under the Creative Commons Attribution-NonCommercial-NoDerivatives 4.0 International License (<http://creativecommons.org/licenses/by-nc-nd/4.0/>).

Reuse

This article is distributed under the terms of the Creative Commons Attribution-NonCommercial-NoDerivatives (CC BY-NC-ND) licence. This licence only allows you to download this work and share it with others as long as you credit the authors, but you can't change the article in any way or use it commercially. More information and the full terms of the licence here: <https://creativecommons.org/licenses/>

Takedown

If you consider content in White Rose Research Online to be in breach of UK law, please notify us by emailing eprints@whiterose.ac.uk including the URL of the record and the reason for the withdrawal request.



eprints@whiterose.ac.uk
<https://eprints.whiterose.ac.uk/>

Information length as a new diagnostic in the periodically modulated double-well model of stochastic resonance

Rainer Hollerbach¹, Eun-jin Kim² and Yanis Mahi^{2,3}

¹*Department of Applied Mathematics,
University of Leeds, Leeds LS2 9JT, U.K.*

²*School of Mathematics and Statistics,
University of Sheffield, Sheffield S3 7RH, U.K.*

³*ENSTA ParisTech, Université Paris-Saclay,
828 Boulevard des Maréchaux, 91120 Palaiseau, France*

Abstract

We consider the classical double-well model of stochastic resonance, in which a particle in a potential $V(x, t) = [-x^2/2 + x^4/4 - A \sin(\omega t) x]$ is subject to an additional stochastic forcing that causes it to occasionally jump between the two wells at $x \approx \pm 1$. We present direct numerical solutions of the Fokker-Planck equation for the probability density function $p(x, t)$, for $\omega = 10^{-2}$ to 10^{-6} , and $A \in [0, 0.2]$. Previous results that stochastic resonance arises if ω matches the average frequency at which the stochastic forcing alone would cause the particle to jump between the wells are quantified. The modulation amplitudes A necessary to achieve essentially 100% saturation of the resonance tend to zero as $\omega \rightarrow 0$. From $p(x, t)$ we next construct the information length $\mathcal{L}(t) = \int [\int (\partial_t p)^2 / p dx]^{1/2} dt$, measuring changes in information associated with changes in p . \mathcal{L} shows an equally clear signal of the resonance, which can be interpreted in terms of the underlying meaning of \mathcal{L} . Finally, we present escape time calculations, where the Fokker-Planck equation is solved only for $x \geq 0$, and find that resonance shows up less clearly than in either the original p or \mathcal{L} .

Highlights:

- Direct numerical solutions of the Fokker-Planck equation governing the classical double-well model of stochastic resonance are presented.
- As $\omega \rightarrow 0$, the amplitudes required to achieve essentially complete synchronization tend to zero as $A \propto 1/|\ln(\pi\sqrt{2}\omega)|$.
- Stochastic resonance has a very clear signature in information length, a recent diagnostic for time-dependent probability density functions.

Keywords:

Stochastic resonance, Fokker-Planck equation, Probability density function, Information geometry

I. INTRODUCTION

Periodically forced systems are common in many different contexts, and can yield large responses through a variety of resonance mechanisms. For example, if a pendulum's support point is oscillated horizontally at the same frequency as its natural frequency, the response will be particularly strong. Alternatively, if the support point is oscillated vertically, the frequency needs to be twice the natural frequency to achieve a so-called parametrically driven resonance. More complicated systems, such as a double-pendulum, have more than one natural frequency, allowing for a range of both directly and parametrically driven resonances as the driving frequency is varied [1].

Next, consider a nonlinear system with more than one equilibrium point, and suppose that the presence of stochastic noise can occasionally cause the system to switch between different equilibria. This introduces a new timescale, namely the average time between successive switching events. However, unlike a pendulum, where every oscillation takes exactly the same time, for stochastic switching events it is only the average time that is a well-defined quantity, but individual events might follow something like a Poisson distribution, and thus have a broad spread about the average value.

Nevertheless, it turns out that even such systems can exhibit what is now known as stochastic resonance. If the driving frequency matches the average switching frequency, then even a small driving amplitude can induce a situation where the switching events no longer have a broad distribution, but instead virtually every switching event is synchronized to the driving, just like a pendulum would be. That is, the noise is playing the rather counter-intuitive role of amplifying the driving signal rather than drowning it out.

The basic mechanism of stochastic resonance was first proposed in 1981 independently by Benzi *et al.* [2] and Nicolis & Nicolis [3], who suggested that it could explain the relatively regular occurrence of ice ages by weak periodic modulations in the Earth's orbital eccentricity. Since this pioneering work, there has been a vast number of further studies [4–11], including applications in physics, chemistry, biology, etc. [12–16], and continuing to this day, e.g. [17–22]. Many different diagnostic quantities have been considered, including the signal-to-noise ratios (especially useful for experimental realizations, e.g. [4, 5]), residence time distributions, and even a variety of information theoretic measures [23–30].

We are here also particularly interested in the information in stochastic systems, how

it changes in time, and how best to measure this. In particular, suppose we have a single stochastic variable x , and we further have its entire probability density function (PDF) $p(x, t)$, giving the probability that x has particular values at time t . Now suppose that p is changing in time. How should one compare two different PDFs, and measure the ‘distance’ between them?

One approach is to use the so-called *information length* \mathcal{L} [31–39], where we first define the PDF’s (time-dependent) correlation time $\tau(t)$ by

$$\mathcal{E}(t) \equiv \frac{1}{\tau^2} = \int \frac{1}{p(x, t)} \left[\frac{\partial p(x, t)}{\partial t} \right]^2 dx, \quad (1)$$

and then

$$\mathcal{L}(t) \equiv \int \frac{dt}{\tau(t)} = \int \sqrt{\int \frac{1}{p(x, t)} \left[\frac{\partial p(x, t)}{\partial t} \right]^2 dx} dt. \quad (2)$$

The interpretation of $\mathcal{L}(t)$ is that it measures the number of statistically distinguishable states that the PDF evolves through in time. Equivalently, the differential element $d\mathcal{L} = dt/\tau(t)$ measures the rate at which new information is being generated during the evolution of p . Note also that \mathcal{L} depends on the entire history between some initial and final times, unlike measures such as Kullback-Leibler divergence [40], which only compares the initial and final PDFs, without any consideration of the intermediate stages. For the periodically forced problem we wish to consider here, \mathcal{L} is then particularly well suited, since it naturally allows us to consider the information change $\Delta\mathcal{L} = \mathcal{L}(t + T) - \mathcal{L}(t)$ over one period T .

The objective of this paper is to reconsider the original Benzi *et al.* model [2] of stochastic resonance, and focus specifically on whether \mathcal{L} per cycle is a useful measure of stochastic resonance, and how it compares with other diagnostics. We start with a direct numerical solution of the associated Fokker-Planck equation, unlike most of the earlier work [6–11] which provided various asymptotic analyses. The numerically computed PDFs $p(x, t)$ already provide direct insight into items such as the probability of being in one or the other of the double-wells, and how this varies throughout the period. From $p(x, t)$ we then further construct the information length \mathcal{L} over a cycle, and find that it is indeed a useful diagnostic for stochastic resonance.

The remainder of this paper is organized as follows. Section 2 introduces the basic model, the associated Fokker-Planck equation, and its numerical solution. Section 3 presents simple diagnostic quantities such as $\int_0^\infty p(x, t) dx$, the probability of being located in $x \geq 0$, and

shows how this can be used to quantify the saturation of the resonance, and how the critical amplitudes A tend to zero as $\omega \rightarrow 0$. Section 4 converts the PDFs to information length per cycle, and shows how this agrees with the previous interpretation of information length, and what the signature of stochastic resonance looks like in \mathcal{L} . Section 5 considers only the half-interval $x \geq 0$, and thus explores how particles escape from a single well. We will see though that this provides a less clear measure of resonance than the measures in Sections 3 and 4. We conclude with a discussion of planned extensions to other stochastic resonance models.

II. DOUBLE-WELL MODEL

Suppose we have a particle in a potential given by

$$V(x, t) = -\frac{x^2}{2} + \frac{x^4}{4} - A \sin(\omega t) x, \quad (3)$$

where x and t are suitably nondimensionalized space and time. If $A = 0$, there are two stable equilibrium points located at $x = \pm 1$, separated by an unstable point at $x = 0$. The potential barrier between the two wells has height $V(0) - V(\pm 1) = 1/4$. For $0 < A \ll 1$, the stable equilibria move as $x \approx \pm 1 + (A/2) \sin(\omega t)$. The depth of the wells also fluctuates as $-1/4 \mp A \sin(\omega t)$ to leading order in A . That is, each well will be slightly deeper than the other one for half of the cycle.

Imagine next that the particle is also subject to stochastic noise, sufficiently great that it can occasionally cause the particle to overcome the potential barrier, and switch from one well to the other. In a frictionally dominated limit, the equation governing the particle's motion can be modelled as

$$\frac{dx}{dt} = -\frac{\partial}{\partial x} V + \xi = x - x^3 + A \sin(\omega t) + \xi, \quad (4)$$

where ξ is a Gaussian-distributed stochastic forcing having the statistical properties

$$\langle \xi(t) \rangle = 0, \quad \langle \xi(t_1) \xi(t_2) \rangle = 2D \delta(t_1 - t_2). \quad (5)$$

That is, ξ has zero mean, is δ -correlated in time, and has strength D .

For the unperturbed $A = 0$ system, the Kramers rate [41] at which such noise would induce switching between the wells is

$$r_K = \frac{1}{\pi\sqrt{2}} \exp\left[-\frac{1}{4D}\right]. \quad (6)$$

Note in particular how r_K tends to zero very quickly as D tends to zero, in agreement with the fact that without noise there would also be no switching at all. This rate r_K is merely an average rate though, with individual switching events exhibiting substantial variation about this average. The question then is whether even a small perturbation A can synchronize the switching so that it precisely follows the externally imposed frequency ω . As we will see below, the answer depends crucially on how the two rates ω and r_K compare with one another. For the right choices of ω and D though, arbitrarily small A can already make the system essentially perfectly synchronized.

Instead of considering the stochastic Langevin equation (4), we will work with the equivalent Fokker-Planck equation [42]

$$\frac{\partial}{\partial t} p(x, t) = -\frac{\partial}{\partial x} \left((x - x^3 + A \sin(\omega t)) p(x, t) \right) + D \frac{\partial^2}{\partial x^2} p(x, t) \quad (7)$$

governing the corresponding probability density function $p(x, t)$. A general analytic solution to this equation is unfortunately not available. A useful limiting case is the adiabatic or quasi-static approximation, in which p is assumed to evolve so slowly that the $\partial_t p$ term can be neglected. The solution then becomes

$$p \propto \exp[-V(x, t)/D], \quad (8)$$

with the constant of proportionality chosen so that $\int_{-\infty}^{+\infty} p dx = 1$. We will see in the next section for which parameter values this adiabatic solution is a valid approximation.

For more general solutions, we resort to a numerical approach. Eq. (7) is discretized using second-order accurate finite differences in both space and time. The interval in x is taken as $x \in [-3, 3]$, which is sufficiently large that simply imposing $p = 0$ boundary conditions at $x = \pm 3$ is an excellent approximation to the original infinite interval. As a useful test, the total probability $\int p dx$ remains constant (=1) to within 10^{-7} . Grid sizes as small as $\Delta x = 10^{-3}$, and time steps as small as $\Delta t = \pi \cdot 10^{-3}$ were chosen, and were varied to check the accuracy.

It is important also to time-step solutions sufficiently long for the final, periodic solutions to emerge. In doing this, care must be taken that the final solution is properly symmetric between the two wells. That is, starting from either (8), or indeed a random initial condition, it is necessary to integrate for only a few periods to obtain a solution that satisfies $p(x, t + T) = p(x, t)$ reasonably well. However, unless it also satisfies $p(x, t + T/2) = p(-x, t)$, there

is still a distinction between the two wells, which the true solution cannot have. And since the timescale to switch between the wells is much longer than the timescale to adjust within each well, many more periods would be needed to achieve a properly symmetric solution.

It was found that this process could be speeded up considerably by adopting the following procedure: time-step for a few periods, use the final values to construct $\tilde{p} = [p(x, t_f) + p(-x, t_f - T/2)]/2$, then use \tilde{p} as a new initial condition. That is, every few periods we simply construct a new initial condition that consists only of the desired symmetric component of the previous results. By repeating this procedure several times, it was found that solutions can be obtained that satisfy both $p(x, t + T) = p(x, t)$ and $p(x, t + T/2) = p(-x, t)$ to within 10^{-6} , and with total integration times up to 100 times shorter than one single integration would have required. Representative samples were checked both ways to ensure that this speed-up procedure really does produce the same final solutions as a single long integration would have. With this speed-up in place, it was then possible to map out the parameter space of interest very thoroughly, even for small ω where the periods $T = 2\pi/\omega$ become rather long.

III. PROBABILITY DENSITY FUNCTIONS

Fig. 1 shows snapshots of the PDFs at the times $t = 0, T/4, T/2$ and $3T/4, \text{mod}(T)$. Only the peaks at $x \approx 1$ are shown; from the symmetry condition $p(x, t + T/2) = p(-x, t)$ the behaviour for $x \approx -1$ is then also known. One immediate point to note is how the peak positions oscillate in time, exhibiting exactly the $(A/2) \sin(\omega t)$ variation expected simply by considering the wells of the potential V . That is, even if the switching between the wells is not necessarily following the adiabatic approximation (8), the behaviour within each well is essentially adiabatic. (For $\omega = O(1)$ the potential does vary so quickly that the PDFs are not adiabatic even within each well; the peak positions then oscillate with an amplitude $A/\sqrt{4 + \omega^2}$, e.g. [12].)

Next, the widths of the PDFs increases with D , as would be expected, since greater noise should broaden the distribution. The precise scaling as $D^{1/2}$ comes from expanding (8) as a Gaussian in the vicinity of the peak position. For $D = 0.01$ the PDFs are indeed very close to Gaussian, but for $D = 0.1$ non-Gaussian behaviour is also clearly present. If D is sufficiently large the PDF spreads out into regions where V can no longer be approximated

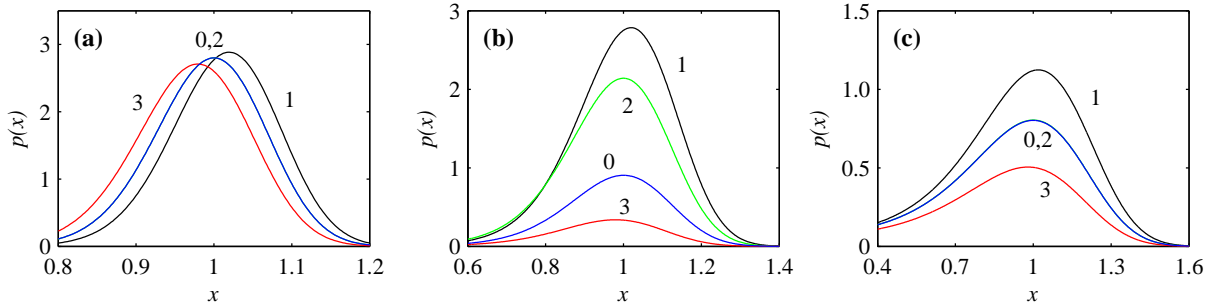


FIG. 1: The PDFs $p(x, t)$ at four times throughout the cycle, with the numbers $n = 0 - 3$ beside individual curves corresponding to $t = nT/4 \bmod(T)$. All three panels are for $\omega = 10^{-4}$ and $A = 0.04$, and (a) $D = 0.01$, (b) $D = 0.0324$, (c) $D = 0.1$.

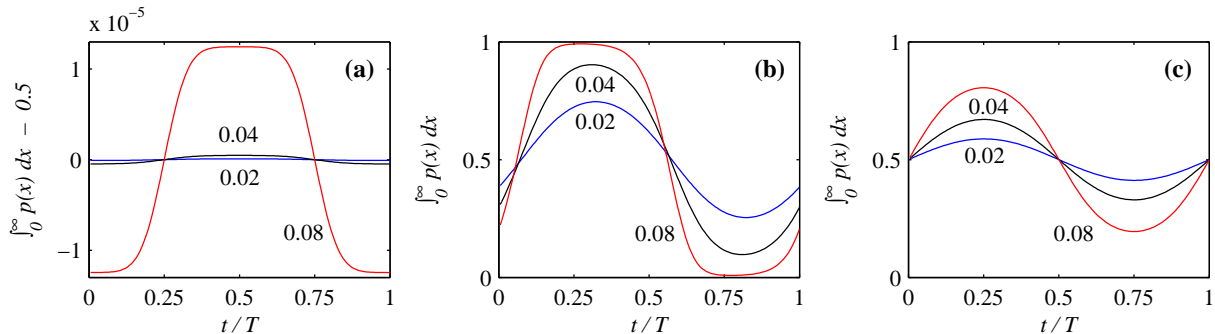


FIG. 2: $\int_0^\infty p(x, t) dx$ as a function of time throughout the period T . All three panels are for $\omega = 10^{-4}$, (a) $D = 0.01$, (b) $D = 0.0324$, (c) $D = 0.1$, and $A = 0.02, 0.04$ and 0.08 as indicated by the numbers beside individual curves. Note also how (a) has a different vertical scale, since deviations from 0.5 never exceed $O(10^{-5})$.

as locally parabolic, which would yield exactly Gaussian behaviour.

Finally, if we compare the amplitudes of p , for $D = 0.01$ they are all broadly similar, whereas for $D = 0.0324$ and 0.1 they are not. Especially for $D = 0.0324$, the PDFs at $t = T/4$ and $3T/4$, and even $t = 0$ and $T/2$, are significantly different, with $t = T/4$ yielding a far higher peak than $t = 3T/4$. From these results it is already clear that $\int_0^\infty p(x, t) dx$, that is, the probability of being located in $x \geq 0$, can vary considerably throughout the cycle. This is quantified in Fig. 2, which shows this probability as a function of time throughout the cycle, for the same solutions as in Fig. 1, as well as A smaller and greater by a factor of 2.

As we can see in Fig. 2, for $D = 0.01$ the deviation from 0.5 barely exceeds 10^{-5} even

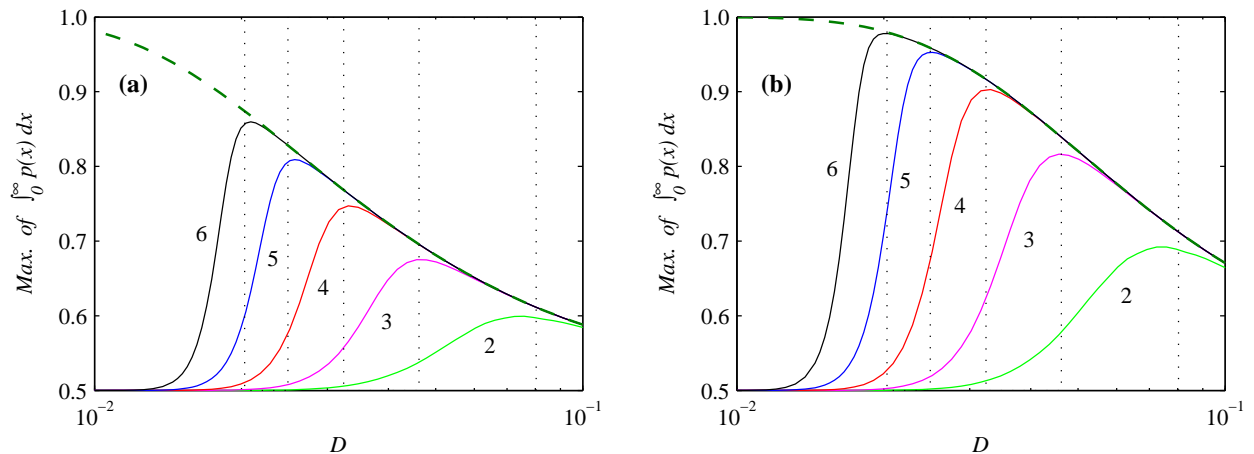


FIG. 3: The maxima over the cycle of $\int_0^\infty p(x, t) dx$, as functions of the noise level D . The numbers 2 to 6 beside individual curves correspond to $\omega = 10^{-2}$ to 10^{-6} . (a) $A = 0.02$, (b) $A = 0.04$. The thick dashed curves show results from (10). The dotted vertical lines are at D_{res} given by (9) for $\omega = 10^{-2}$ to 10^{-6} ; note how well these values agree with the maxima over D of the corresponding curves.

for $A = 0.08$. That is, even a relatively large modulation has almost no effect on the probability of being located in one well versus the other, even at those times in the cycle when a given well ‘should’ be preferred, in the sense that it is deeper than the other one. In contrast, for $D = 0.0324$ and 0.1 even the relatively small modulation $A = 0.02$ is already enough to induce clear deviations from 0.5 . For $D = 0.0324$ and $A = 0.08$ the probability of being located in $x \geq 0$ at $t = T/4$ even exceeds 0.99 . That is, the switching process is essentially saturated, and perfectly synchronized with the periodic forcing, with virtually 100% probability of being located in $x \geq 0$ at $t = T/4$, and correspondingly in $x \leq 0$ at $t = 3T/4$.

We thus recognize that the most important diagnostic quantity to understand the resonant behaviour is the maximum over the cycle of $\int_0^\infty p(x, t) dx$. Fig. 3 shows this quantity, for $\omega = 10^{-2}$ to 10^{-6} , and $D \in [0.01, 0.1]$. The pattern is very clear: if D is too small, this maximum remains essentially 0.5 , indicating that there is no preference for one well over the other at any time in the cycle, and hence no synchronization. For larger D however, the values suddenly rise and then slowly decrease again. For smaller ω the rise is more abrupt, and occurs at smaller values of D . For the gradual decrease after the maximum value has been reached, all frequencies ω converge to the same curve.

To understand these results, we start by equating $\omega = r_K$. Solving $\omega = \exp(-1/4D)/(\pi\sqrt{2})$ for D yields

$$D_{\text{res}} = \frac{-1}{4 \ln(\pi\sqrt{2}\omega)}, \quad (9)$$

where the subscript ‘res’ indicates that this is the resonant value. In particular, we see in Fig. 3 that the maxima of the individual ω curves all occur very close to their corresponding D_{res} values.

Next, the thick dashed lines in Fig. 3 show the equivalent results for the adiabatic expression (8). That is, we are interested in the quantity

$$\int_0^\infty \exp[-V(x, T/4)/D] dx \Big/ \int_{-\infty}^{+\infty} \exp[-V(x, T/4)/D] dx. \quad (10)$$

Analytic expressions for these integrals do not exist, but they can be evaluated numerically to yield the curves shown in Fig. 3. An asymptotic formula can also be obtained by noting that the PDFs are concentrated within the wells of V , especially for small D , and at $t = T/4$ the wells have depths $-1/4 \mp A$. If we approximate the integrals simply by the peak values of the integrands, the asymptotic formula becomes

$$\frac{\exp[(1/4 + A)/D]}{\exp[(1/4 + A)/D] + \exp[(1/4 - A)/D]} = \frac{1}{1 + \exp[-2A/D]}, \quad (11)$$

which differs from the numerically computed value by only a few percent even for $D = 0.1$, with even better agreement as D is decreased.

We can then summarize Fig. 3 as follows: First, if $D \ll D_{\text{res}}$, then $\omega \gg r_K$. The imposed modulation is then too rapid, the system cannot effectively respond, and the probability of being in either well remains essentially 0.5 throughout the entire cycle. That is, there is no synchronization between the stochastic switching and the modulation, and hence no resonance. In contrast, if $D \gg D_{\text{res}}$, then $\omega \ll r_K$. The imposed modulation is then so slow that the adiabatic limit (8) does indeed apply, even to a process as slow as the switching between the wells. And as the results from (10) or (11) show, the adiabatic formula (8) exhibits synchronization, and in particular stronger synchronization for smaller D , explaining why D should be as small as possible, but not much less than D_{res} , which would switch the resonance off.

An immediate consequence of these results is also that a resonant peak occurs only if a scan is done over the noise level D , as here. If instead D is held fixed and a scan is done

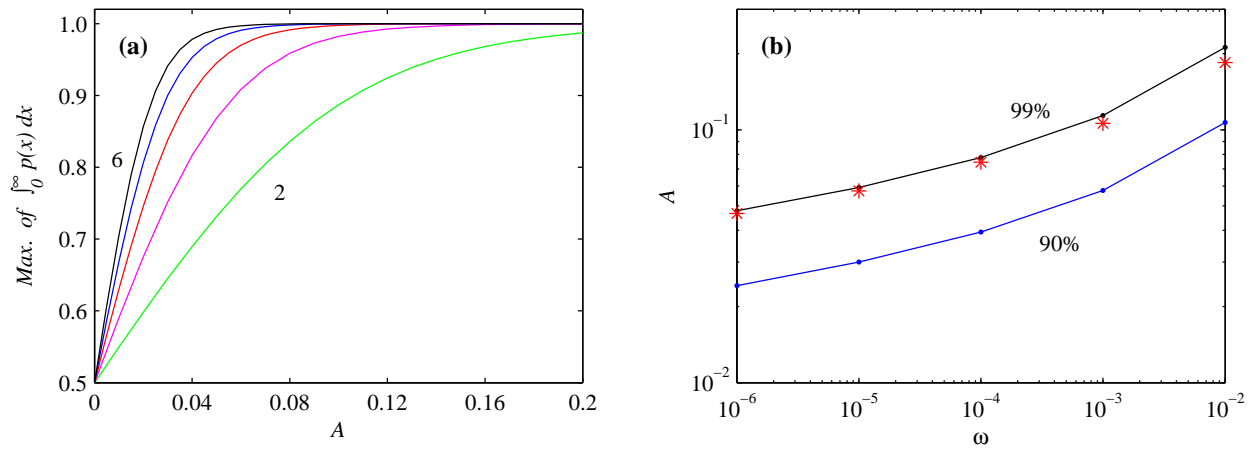


FIG. 4: (a) The maximum over the cycle of $\int_0^\infty p(x, t) dx$ as a function of the modulation amplitude A . The numbers 2 and 6 indicate the range $\omega = 10^{-2}$ to 10^{-6} . For each ω , $D = D_{\text{res}}$. (b) The critical values of A required for the maxima in (a) to equal 0.9 for the lower curve, and 0.99 for the upper curve, corresponding to 90% and 99% probabilities of being in the ‘correct’ well. The asterisks correspond to $A = 2.3 D$, with $D = D_{\text{res}}$ again given by (9).

over ω , then the ‘resonance’ becomes a simple on-off phenomenon: if $\omega \gg r_K$ there is no synchronization, whereas if $\omega \ll r_K$ there is synchronization, at whatever level (10) yields for the given D (and A), but no variation with ω , since (10) does not involve ω .

Fig. 4 quantifies how the resonance saturates as the modulation amplitude A is increased. That is, for a given ω , suppose we first fix D at its resonant value D_{res} , and then gradually increase A . How does the maximum value of $\int_0^\infty p(x, t) dx$ over the cycle increase, and how large would A therefore have to be to have, say, 90% or 99% probability of being in the ‘correct’ well at the appropriate time in the cycle? Fig. 4a shows the overall variation with A , whereas Fig. 4b picks out the particular A values where the probability equals 0.9 and 0.99. As we can see in Fig. 4b, the amplitudes required to achieve even 99% probability decrease as ω decreases. Also shown is the asymptotic formula $A = 2.3 D$, which is seen to be an excellent fit. This result is readily understood from (11); $1/(1 + \exp(-2A/D)) = 0.99$ yields $A = 2.3 D$. For sufficiently small ω , and corresponding D_{res} , the stochastic resonance phenomenon therefore becomes increasingly efficient, and essentially 100% synchronization can be achieved even at very small modulation amplitudes, tending to zero as $O(D)$.

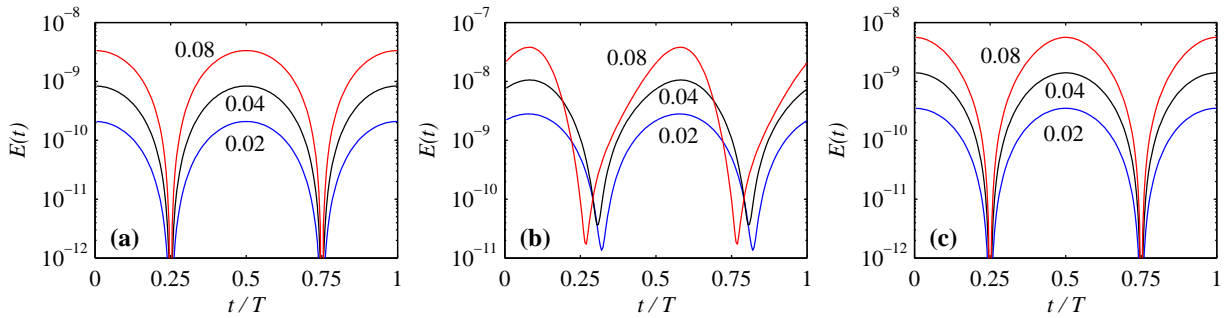


FIG. 5: $\mathcal{E}(t)$ as a function of time throughout the period T . All three panels are for $\omega = 10^{-4}$, (a) $D = 0.01$, (b) $D = 0.0324$, (c) $D = 0.1$, and $A = 0.02, 0.04$ and 0.08 as indicated by the numbers beside individual curves.

IV. INFORMATION LENGTH

Having established what the basic resonance phenomenon looks like in terms of the PDFs directly, we turn next to the diagnostic quantities \mathcal{E} and \mathcal{L} from Eqs. (1) and (2). Fig. 5 shows \mathcal{E} for the previous solutions from Figs. 1 and 2. Recalling that the position of the peaks varies as $(A/2)\sin(\omega t)$, we see that \mathcal{E} is consistently greatest when the peaks are moving fastest. The greatest values of \mathcal{E} are for the intermediate case $D = 0.0324$, in agreement with Fig. 2b for example. On the other hand, unlike Figs. 2a and 2c, which had very different magnitudes, here the values in Figs. 5a and 5c are quite similar. It is clear therefore that Fig. 5 is measuring something different from Fig. 2. In particular, whereas Fig. 2 only encapsulates the probability to be in one well or the other, Fig. 5 also includes the information about how the PDFs move back and forth within a given well.

Fig. 6 shows the information length \mathcal{L} per cycle associated with the results from Fig. 3. We see that \mathcal{L} exhibits a beautiful signal of the resonance phenomenon, just as clear as the probabilities themselves. To interpret these results, we start with the thick dashed lines, which are simply $4A/1.4D^{1/2}$. To understand the significance of this formula, we first recall that the peaks move according to $(A/2)\sin(\omega t)$. The total distance each peak moves throughout a cycle is therefore $2A$. Next, the two PDF peaks at $x \approx \pm 1$ each have standard deviation $\sigma \approx \sqrt{D/2}$, with the approximation becoming better for smaller D , where the peaks are increasingly close to Gaussian (Fig. 1). The width of each peak is therefore $2\sigma = 1.4D^{1/2}$. (As we can also see in Fig. 1, the width actually varies slightly throughout the period, but to obtain a lowest order estimate of what \mathcal{L} should be, just the average

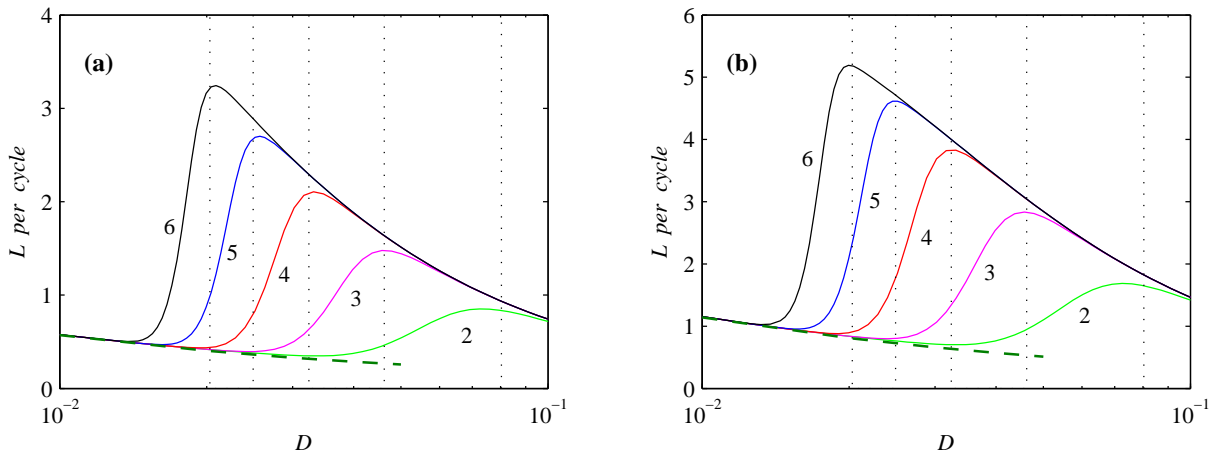


FIG. 6: \mathcal{L} over one cycle, as functions of the noise level D . The numbers 2 to 6 beside individual curves correspond to $\omega = 10^{-2}$ to 10^{-6} . (a) $A = 0.02$, (b) $A = 0.04$. The thick dashed curves are $\mathcal{L} = 4A/1.4D^{1/2}$. As in Fig. 3, the dotted vertical lines are at D_{res} given by (9) for $\omega = 10^{-2}$ to 10^{-6} ; note how well these values again agree with the maxima of the corresponding curves.

width is sufficient.) So, if each peak moves a total distance $2A$, and has width $1.4D^{1/2}$, then the number of statistically distinguishable states it moves through is just $2A/1.4D^{1/2}$. The final factor of 2 is simply due to the fact that there are two peaks, each undergoing the same motion. We see therefore that in this small D regime before the resonance sets in, \mathcal{L} is measuring precisely the motion of the peaks, and there is no other source of information length.

The sudden increase in \mathcal{L} as the resonance sets in is then measuring the additional information, and associated number of statistically distinguishable states, that comes from the synchronization behaviour, as the probability of being in one well or the other at the appropriate times in the cycle becomes significantly different from 0.5. Finally, for D sufficiently large that \mathcal{L} is decreasing again, it decreases more rapidly than the previous $D^{-1/2}$ scaling. The reason for this is that in addition to the previous $D^{-1/2}$ factor (which we recall comes from the broadening of the peaks, and thus continues to apply), the contribution from the synchronization also decreases again, since according to Fig. 3 the synchronization itself decreases once the solutions are firmly on the adiabatic curve (10).

Fig. 7 shows the information length associated with the saturation results in Fig. 4a. Unlike the probabilities, which are necessarily bounded to remain below 100%, \mathcal{L} can and

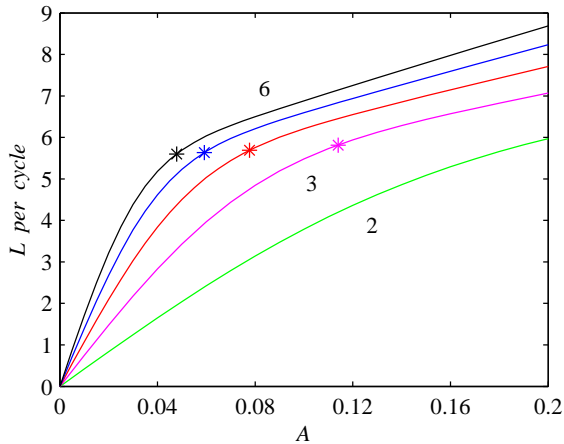


FIG. 7: The \mathcal{L} values corresponding to the results in Fig. 4a, again as functions of the modulation amplitude A . The numbers beside curves again indicate the range $\omega = 10^{-2}$ to 10^{-6} . For each ω , $D = D_{\text{res}}$. The asterisks on the 3 to 6 curves correspond to the 99% values in Fig. 4b, indicating the transition in \mathcal{L} as a function of A once the resonance is essentially fully saturated.

does continue to increase even after the probabilities have saturated. We see though that the slope of the \mathcal{L} versus A curves decreases significantly, right around the point where the probabilities reach 99%. This again illustrates the intuitive interpretation of \mathcal{L} as a measure of the information changes in the PDF. Before the probabilities have saturated, \mathcal{L} is increasing both due to the increasing $(A/2)\sin(\omega t)$ motion of the peaks, and due to the increasing degree of synchronization, whereas after the synchronization is complete it is only the peaks' motion that can continue to increase, and hence cause \mathcal{L} to increase.

V. ESCAPE TIMES

Another tool that has been used in the past [6, 43–48] to study stochastic resonance is to investigate the escape of particles from a single well. That is, suppose we solve the same Fokker-Planck equation (7) as before, but now only on the interval $x \in [0, 3]$. The boundary condition at $x = 0$ is $p = 0$, meaning that any particles that reach $x = 0$ are simply lost to the system. And indeed, the ‘total probability’ integral, $\int p(x, t) dx$, no longer remains constant in this formulation, but instead decreases in time, corresponding to the continual loss of particles at $x = 0$. The question then is, can we analyze and interpret this loss of

particles in a similar way to the previous results, and in particular can we see the signature of resonance here as well?

Starting from some suitable peak within the $x \approx 1$ well, integrating for just a few periods yields a solution that is again periodic in time, but now also decreases by a constant factor each period. That is, the solutions are of the form $p(x, t+T) = c p(x, t)$, where $c < 1$ is some factor that depends on the parameters D , ω and A , but is the same for each subsequent period once this behaviour has emerged. Also, because there is now only one well, the previous symmetrization procedure does not need to be applied, and this behaviour still arises after just a few periods.

Note also that this initialization procedure is deliberately chosen to erase all knowledge of the precise initial condition that was originally used. In contrast, it can also be very interesting to study escape times for specific initial conditions at particular times in the cycle, e.g. [49–53], but such results are less directly comparable to the results in Sections 3 and 4, where the initial conditions also do not matter.

Fig. 8 shows this reduction by a constant factor each period, starting from such initialized solutions (rescaled so that they start out with $\int p dx = 1$ again). The top row shows $G(t) = \int_0^\infty p(x, t) dx$, that is, a measure of the number of particles left. The bottom row shows $W(t) = -\frac{d}{dt}G(t)$, corresponding to the rate at which particles are lost. For all choices of D and A , the pattern is as asserted above, with both G and W decreasing by the same factor c in each successive period. We see furthermore that increasing either D or A yields a smaller c ; that is, the particles are lost more quickly. This is hardly surprising; greater noise or greater periodic modulation should indeed both promote faster loss of particles.

The other interesting feature to note in Fig. 8 is that the losses $W(t)$ occur in bursts, strongly concentrated in the times between $t = T/2$ and $T, \text{ mod}(T)$, with far less lost in the other half of the cycle. This is again as expected; depending on whether the well is shallower or deeper, particles are more or less likely to be lost. To quantify this effect, it is convenient to split the overall reduction factor into two separate factors as $c = R_1 R_2$, with $R_{1,2}$ defined by

$$R_1 \equiv \frac{G(T/2)}{G(0)}, \quad R_2 \equiv \frac{G(T)}{G(T/2)}, \quad (12)$$

with all times $\text{mod}(T)$. The bursting behaviour then means that $R_2 < R_1$, and ideally we would like R_1 to remain as close to 1 as possible, while simultaneously having $R_2 \ll 1$. This would be the closest equivalent to the previous synchronization in Fig. 3, since it would

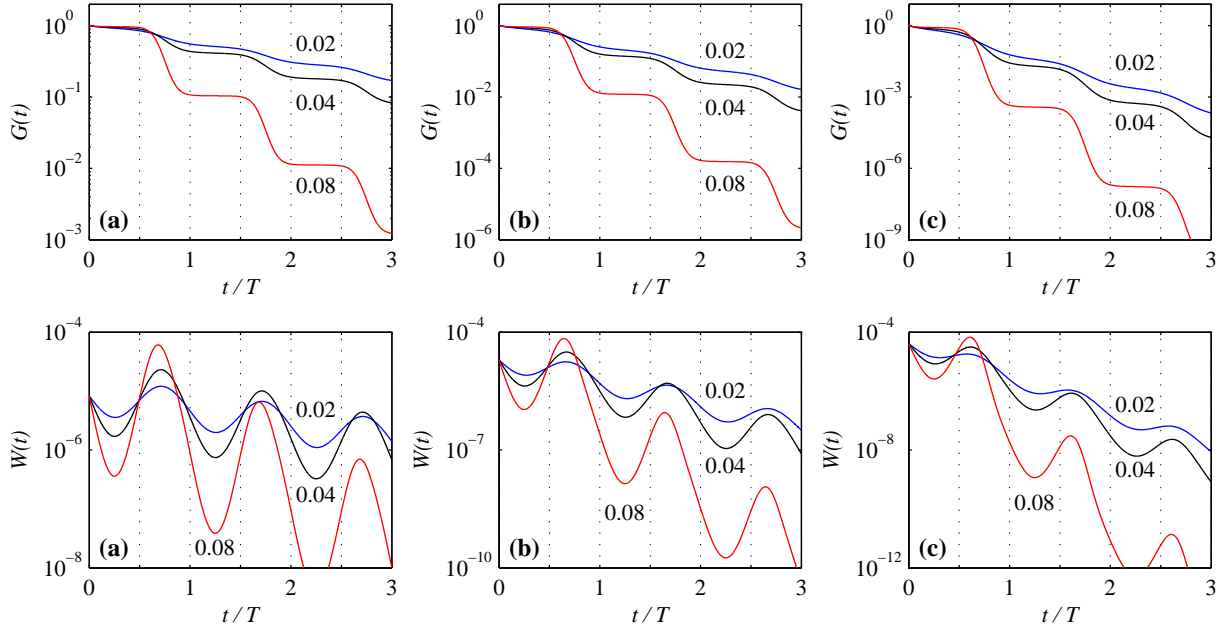


FIG. 8: The top row shows $G(t) = \int_0^\infty p(x, t) dx$, and the bottom row the corresponding $W(t) = -\frac{d}{dt}G(t)$. All three solutions are for $\omega = 10^{-4}$, (a) $D = 0.023$, (b) $D = 0.025$, (c) $D = 0.027$, and $A = 0.02, 0.04$ and 0.08 as indicated by the numbers beside individual curves.

mean that almost nothing is lost during the favourable part of the cycle, but then almost everything is lost during the unfavourable part.

Fig. 9 shows how the reduction factors R_1 and R_2 vary with D , ω and A . We see again the previous result that increasing D increases the losses, that is, yields smaller R_1 and R_2 . Increasing A decreases R_2 , but increases R_1 . That is, it increases the contrast between the favourable versus unfavourable parts of the cycle, which is indeed exactly what increasing A corresponds to. Finally, regarding the variation with ω , we note that the transition point where $R_{1,2}$ still close to 1 gives way to $R_{1,2} \ll 1$ is broadly consistent with the previous D_{res} relationship (9) between ω and D . However, unlike Figs. 3 or 6, where there were definite maxima in the curves that allowed an unambiguous definition of the ‘resonance’ point, here there is no clear identification of what would be the ‘best’ noise level. We conclude therefore that escape time calculations such as these are consistent with the basic stochastic resonance phenomenon, but that the calculations of Sections 3 and 4 allow a more precise definition.

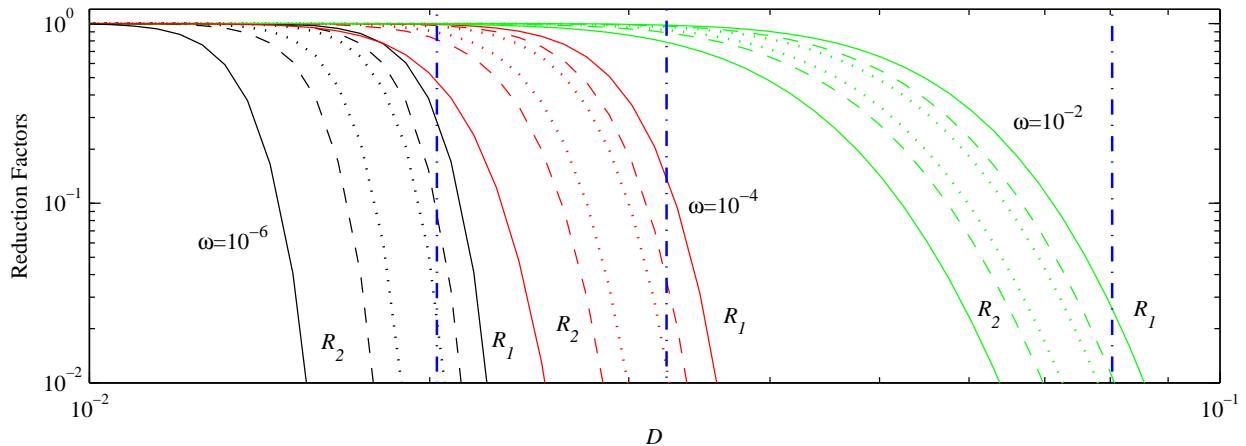


FIG. 9: The reduction factors R_1 and R_2 in Eq. (12), as functions of the noise level D , and $\omega = 10^{-2}$, 10^{-4} and 10^{-6} as labelled. Within each set of six curves the innermost, dotted ones are for $A = 0.02$, the dashed curves are for $A = 0.04$, and the outermost, solid ones are for $A = 0.08$. The vertical dash-dotted lines are at $D = 0.0203$, 0.0324 , and 0.0803 , namely D_{res} for the given ω values.

VI. CONCLUSION

We investigated the phenomenon of stochastic resonance by direct numerical solutions of the governing Fokker-Planck equation, and found that it can be precisely quantified by considering the probability to be in one well or the other at the appropriate parts of the cycle. We showed that if the noise level D is taken as the resonant value D_{res} for a given frequency ω , then in the limit $\omega \rightarrow 0$, the modulation amplitude A can also become arbitrarily small while still achieving essentially 100% synchronization of the switching with the modulation. We furthermore showed that information length \mathcal{L} is a useful diagnostic tool for this problem, with a very clear signature of the resonance emerging.

In contrast, comparisons of different PDFs that do not involve their entire evolution histories, such as Kullback-Leibler divergence [40], would probably not be useful for problems such as this, where the PDFs evolve periodically in time. That is, if a diagnostic tool that simply compares two PDFs at two different times is applied to times t and $t + T$, where the PDFs are the same, the results cannot say anything about the actual evolution over the period T . See also [38], who suggest that information length is more useful than Kullback-Leibler divergence even in systems that are not periodic in time.

Finally, future extensions of this work include stochastic resonance in two (or more) coupled variables [54–59], periodic modulations in the noise levels rather than the potential V [60–65], and molecular motors, where the potential V is periodic in space as well as time [66–68].

-
- [1] M. Gitterman, *The Chaotic Pendulum*, World Scientific, 2010.
 - [2] R. Benzi, A. Sutera, A. Vulpiani, The mechanism of stochastic resonance, *J. Phys. A* 14 (1981) L453-457.
 - [3] C. Nicolis, G. Nicolis, Stochastic aspects of climate transitions - additive fluctuations, *Tellus* 33 (1981) 225-234.
 - [4] S. Fauve, F. Heslot, Stochastic resonance in a bistable system, *Phys. Lett.* 97 (1983) 5-7.
 - [5] B. McNamara, K. Wiesenfeld, R. Roy, Observation of stochastic resonance in a ring laser, *Phys. Rev. Lett.* 60 (1988) 2626-2629.
 - [6] L. Gammaitoni, F. Marchesoni, E. Menichella-Saetta, S. Santucci, Stochastic resonance in bistable systems, *Phys. Rev. Lett.* 62 (1989) 349-352.
 - [7] R.F. Fox, Stochastic resonance in a double well, *Phys. Rev. A* 39 (1989) 4148-4153.
 - [8] B. McNamara, K. Wiesenfeld, Theory of stochastic resonance, *Phys. Rev. A* 39 (1989) 4854-4869.
 - [9] P. Jung, P. Hänggi, Stochastic nonlinear dynamics modulated by external periodic forces, *EPL* 8 (1989) 505-510.
 - [10] Hu Gang, G. Nicolis, C. Nicolis, Periodically forced Fokker-Planck equation and stochastic resonance, *Phys. Rev. A* 42 (1990) 2030-2041.
 - [11] P. Jung, P. Hänggi, Amplification of small signals via stochastic resonance, *Phys. Rev. A* 44 (1991) 8032-8042
 - [12] P. Jung, Periodically driven stochastic systems, *Phys. Rep.* 234 (1993) 175-295.
 - [13] L. Gammaitoni, P. Hänggi, P. Jung, F. Marchesoni, Stochastic resonance, *Rev. Mod. Phys.* 70 (1998) 223-287.
 - [14] P. Hänggi, Stochastic resonance in biology: How noise can enhance detection of weak signals and help improve biological information processing, *ChemPhysChem* 3 (2002) 285-290.
 - [15] T. Wellens, V. Shatokhin, A. Buchleitner, Stochastic resonance, *Rep. Prog. Phys.* 67 (2004)

- [16] F. Sagués, J.M. Sancho, J. Garcia-Ojalvo, Spatiotemporal order out of noise, *Rev. Mod. Phys.* 79 (2007) 829-882.
- [17] R. Ren, M. Luo, K. Deng, Stochastic resonance in a fractional oscillator driven by multiplicative quadratic noise, *J. Stat. Mech.* 2017 (2017) 023210.
- [18] C.-J. Wang, F. Long, P. Zhang, L.-R. Nie, Controlling of stochastic resonance and noise enhanced stability induced by harmonic noises in a bistable system, *Physica A* 471 (2017) 288-294.
- [19] G. He, D. Guo, Y. Tian, T. Li, M. Luo, Mittag-Leffler noise induced stochastic resonance in a generalized Langevin equation with random inherent frequency, *Physica A* 484 (2017) 91-103.
- [20] C. Nicolis, G. Nicolis, Coupling-enhanced stochastic resonance, *Phys. Rev. E* 96 (2017) 042214.
- [21] P. Xu, Y. Jin, Stochastic resonance in multi-stable coupled systems driven by two driving signals, *Physica A* 492 (2018) 1281-1289.
- [22] S. Mondal, J. Das, B.C. Bag, F. Marchesoni, Autonomous stochastic resonance driven by colored noise, *Phys. Rev. E* 98 (2018) 012120.
- [23] C. Heneghan, C.C. Chow, J.J. Collins, T.T. Imhoff, S.B. Lowen, M.C. Teich, Information measures quantifying aperiodic stochastic resonance, *Phys. Rev. E* 54 (1996) R2228-2231.
- [24] J.W.C. Robinson, D.E. Asraf, A.R. Bulsara, M.E. Inchiosa, Information-theoretic distance measures and a generalization of stochastic resonance, *Phys. Rev. Lett.* 81 (1998) 2850-2853.
- [25] I. Goychuk, P. Hänggi, Stochastic resonance in ion channels characterized by information theory, *Phys. Rev. E* 61 (2000) 4272-4280.
- [26] I. Goychuk, Information transfer with rate-modulated Poisson processes: A simple model for nonstationary stochastic resonance, *Phys. Rev. E* 64 (2001) 21909.
- [27] M.D. McDonnell, N.G. Stocks, C.E.M. Pearce, D. Abbott, *Stochastic Resonance: From Suprathreshold Stochastic Resonance to Stochastic Signal Quantization*, Cambridge University Press, 2008.
- [28] I. Goychuk, P. Hänggi, Nonstationary stochastic resonance viewed through the lens of information theory, *Europ. Phys. J. B* 69 (2009) 29-35.
- [29] B. Meyer, Optimal information transfer and stochastic resonance in collective decision making, *Swarm Intelligence* 11 (2017) 131-154.
- [30] N. Gillard, E. Belin, F. Chapeau-Blondeau, Enhancing qubit information with quantum ther-

- mal noise, *Physica A* 507 (2018) 219-230.
- [31] S.B. Nicholson, E. Kim, Investigation of the statistical distance to reach stationary distributions, *Phys. Lett. A* 379 (2015) 83-88.
- [32] J. Heseltine, E. Kim, Novel mapping in non-equilibrium stochastic processes, *J. Phys.* 49 (2016) 175002.
- [33] E. Kim, U. Lee, J. Heseltine, R. Hollerbach, Geometric structure and geodesic in a solvable model of nonequilibrium process, *Phys. Rev. E* 93 (2016) 062127.
- [34] S. Nicholson, E. Kim, Structures in sound: Analysis of classical music using the information length, *Entropy* 18 (2016) 258.
- [35] L.-M. Tenkès, R. Hollerbach, E. Kim, Time-dependent probability density functions and information geometry in stochastic logistic and Gompertz models, *J. Stat. Mech.* 2017 (2017) 123201.
- [36] E. Kim, P. Lewis, Information length in quantum systems, *J. Stat. Mech.* 2018 (2018) 043106.
- [37] E. Kim, Investigating information geometry in classical and quantum systems through information length, *Entropy* 20 (2018) 574.
- [38] Q. Jacquet, E. Kim, R. Hollerbach, Time-dependent probability density functions and attractor structure in self-organised shear flows, *Entropy* 20 (2018) 613.
- [39] H. Suzuki, Y. Hashizume, Expectation parameter representation of information length for non-equilibrium systems, *Physica A* 517 (2019) 400-408.
- [40] B.R. Frieden, *Science from Fisher Information*, Cambridge University Press, 2004.
- [41] H.A. Kramers, Brownian motion in a field of force and the diffusion model of chemical reactions, *Physica* 7 (1940) 284-304.
- [42] H. Risken, *The Fokker-Planck Equation: Methods of Solution and Applications*, Springer, 1996.
- [43] T. Zhou, F. Moss, P. Jung, Escape-time distributions of a periodically modulated bistable system with noise, *Phys. Rev. A* 42 (1990) 3161-3169
- [44] J.M. Casado, M. Morillo, Distribution of escape times in a driven stochastic model, *Phys. Rev. E* 49 (1994) 1136-1139.
- [45] J. Kallunki, M. Dubé, T. Ala-Nissila, Stochastic resonance and diffusion in periodic potentials, *J. Phys. Cond. Matter* 11 (1999) 9841-9849.
- [46] F. Pétrélis, S. Aumaître, K. Mallick, Escape from a potential well, stochastic resonance and

- zero frequency component of the noise, *EPL* 79 (2007) 40004.
- [47] Y. Hasegawa, M. Arita, Escape process and stochastic resonance under noise intensity fluctuation, *Phys. Lett. A* 375 (2011) 3450-3458.
 - [48] W. Wang, Z. Yan, X. Liu, The escape problem and stochastic resonance in a bistable system driven by fractional Gaussian noise, *Phys. Lett. A* 381 (2017) 2324-2336.
 - [49] P. Reimann, G.J. Schmid, P. Hänggi, Universal equivalence of mean first-passage time and Kramers rate, *Phys. Rev. E* 60 (1999) R1-4.
 - [50] J. Lehmann, P. Reimann, P. Hänggi, Surmounting oscillating barriers, *Phys. Rev. Lett.* 84 (2000) 1639-1642.
 - [51] J. Lehmann, P. Reimann, P. Hänggi, Surmounting oscillating barriers: Path-integral approach for weak noise, *Phys. Rev. E* 62 (2000) 6282-6303.
 - [52] M. Schindler, P. Talkner, P. Hänggi, Firing time statistics for driven neuron models: Analytic expressions versus numerics, *Phys. Rev. Lett.* 93 (2004) 048102.
 - [53] P. Talkner, L. Machura, M. Schindler, P. Hänggi, J. Luczka, Statistics of transition times, phase diffusion and synchronization in periodically driven bistable systems, *New J. Phys.* 7 (2005) 014.
 - [54] P. Jung, U. Behn, E. Pantazelou, F. Moss, Collective response in globally coupled bistable systems, *Phys. Rev. A* 46 (1992) R1709-1712.
 - [55] J.F. Lindner, B.K. Meadows, W.L. Ditto, M.E. Inchiosa, A.R. Bulsara, Array enhanced stochastic resonance and spatiotemporal synchronization, *Phys. Rev. Lett.* 75 (1995) 3-6.
 - [56] A. Pikovsky, A. Zaikin, M.A. De la Casa, System size resonance in coupled noisy systems and in the Ising model, *Phys. Rev. Lett.* 88 (2002) 506011.
 - [57] S.F. Huelga, M.B. Plenio, Stochastic resonance phenomena in quantum many-body systems, *Phys. Rev. Lett.* 98 (2007) 170601.
 - [58] G. Harras, C.J. Tessone, D. Sornette, Noise-induced volatility of collective dynamics, *Phys. Rev. E* 85 (2012) 011150.
 - [59] A. Rosas, D. Escaff, I.L.D. Pinto, K. Lindenberg, Globally coupled stochastic two-state oscillators: Synchronization of infinite and finite arrays, *J. Phys. A* 49 (2016) 095001.
 - [60] L. Gammaitoni, F. Marchesoni, E. Menichella-Saetta, S. Santucci, Multiplicative stochastic resonance, *Phys. Rev. E* 49 (1994) 4878-4881.
 - [61] V. Berdichevsky, M. Gitterman, Multiplicative stochastic resonance in linear systems: Ana-

- lytical solution, EPL 36 (1996) 161-165.
- [62] W.-R. Zhong, Y.-Z. Shao, Z.-H. He, Pure multiplicative stochastic resonance of a theoretical anti-tumor model with seasonal modulability, Phys. Rev. E 73 (2006) 060902.
- [63] L.-C. Du, D.-C. Mei, Stochastic resonance induced by a multiplicative periodic signal in a bistable system with cross-correlated noises and time delay, J. Stat. Mech. 2008 (2008) P11020.
- [64] T. Srokowsky, Nonlinear stochastic equations with multiplicative Lévy noise, Phys. Rev. E 81 (2010) 051110.
- [65] A. Rosas, I.L.D. Pinto, K. Lindenberg, Kramers' rate for systems with multiplicative noise, Phys. Rev. E 94 (2016) 012101.
- [66] F. Jülicher, A. Ajdari, J. Prost, Modeling molecular motors, Rev. Mod. Phys. 69 (1997) 1269-1281.
- [67] X.-J. Zhang, H. Qian, M. Qian, Stochastic theory of nonequilibrium steady states and its applications, Phys. Rep. 510 (2012) 1-86.
- [68] H. Qian, Cooperativity in cellular biochemical processes: Noise-enhanced sensitivity, fluctuating enzyme, bistability with nonlinear feedback, and other mechanisms for sigmoidal responses, Ann. Rev. Biophys. 41 (2012) 179-204.